applied optics

Characterization of drying paint coatings by dynamic speckle and holographic interferometry measurements

N. Budini,[1,2,*] C. Mulone,[3] N. Balducci,[3] F. M. Vincitorio,[3] A. J. López,[4] and A. Ramil[4]

[1]Instituto de Física del Litoral (IFIS Litoral, UNL-CONICET), Güemes 3450, S3000GLN Santa Fe, Argentina
[2]Departamento de Física, Facultad de Ingeniería Química (UNL), Sgo. del Estero 2829, S3000AOM Santa Fe, Argentina
[3]Universidad Tecnológica Nacional, Facultad Regional Paraná, Av. Almafuerte 1033, E3100XAI Paraná, Entre Ríos, Argentina
[4]Universidade da Coruña, Centro de Investigacións Tecnolóxicas, Campus de Esteiro S/N, 15403 Ferrol, Spain
*Corresponding author: nicolas.budini@ifis.santafe-conicet.gov.ar

Received 21 March 2016; revised 11 May 2016; accepted 16 May 2016; posted 18 May 2016 (Doc. ID 261501); published 7 June 2016

In this work we implemented dynamic speckle and holographic interferometry techniques to characterize the drying process of solvent-based paint coatings. We propose a simple way to estimate drying time by measuring speckle activity and incrementally fitting experimental data through standard regression algorithms. This allowed us to predict drying time after about 20–30 min of paint application, which is fast compared to usual times required to reach the so-called tack-free state (≈2 h). In turn, we used holographic interferometry to map small thickness variations in the coating surface during drying. We also demonstrate that results obtained from both techniques correlate with each other, which allows us to improve the accuracy of the drying time estimation.

OCIS codes: (120.4290) Nondestructive testing; (310.1515) Protective coatings; (120.2880) Holographic interferometry; (120.6150) Speckle imaging.

http://dx.doi.org/10.1364/AO.55.004706

1. INTRODUCTION

Paint coatings serve diverse purposes in a variety of domestic, scientific, and industrial applications. Paints are used to improve the appearance, durability, resistance, protection against corrosion, and other qualities of many materials [1]. The ability to characterize the drying process of paint coatings after their application is relevant in the context of paint manufacture, application, and quality optimization [2,3].

Several works have been devoted to analyzing the drying process of paints. Most of them implemented dynamic speckle techniques, like speckle interferometry [2,4] or dynamic speckle correlation [3,5–8]. In small proportion, other works employed methods based on digital holographic interferometry (DHI) [1,9]. Dynamic speckle methods represent a very straightforward alternative for analyzing the drying process of paints, since the experimental setup is quite simple and speckle activity (SA) is a qualitative descriptor that can be directly related to the degree of stiffness of a drying paint coating [10]. On the other hand, the high sensitivity of the DHI technique in detecting shape variations makes observation and analysis of the complete drying process of paints somewhat more complicated. At the same time, however, this allows the use of DHI to inspect the last stages of the drying process in a very precise manner by mapping small shape variations of coatings while they dry completely.

Despite the fact that both techniques mentioned have already been applied separately to analyze the drying process of paint coatings [1–10], they have never been implemented at the same time to exploit their combination or to correlate their results. Moreover, attending to the separate implementation of both techniques, no work is found in the literature to date regarding either drying time prediction through fitting of experimental SA values as they are acquired or quantification of shape or thickness variations of drying coatings through DHI.

Therefore, in this work we have implemented both dynamic speckle and DHI techniques to analyze and characterize the drying process of solvent-based paints. In the context of this work, the characterization involved estimating drying time during the first stages of drying and determining small thickness variations of the paint coating as it dried completely. We propose a simple way to estimate drying time by measuring SA and incrementally fitting acquired data through standard regression (Section 4.A). As will be shown, this allowed us to predict drying time after about 20–30 min of paint application, which is faster than the time the paint needs to reach the so-called tack-free or surface dry state (about 2 h for solvent-based paints,

depending on ambient conditions) [2]. We also show, for the first time to our knowledge, the application of the DHI technique to map and quantify thickness variations of paint coatings during the last stages of the drying process (Section 4.B). Finally, we demonstrate that results from both techniques correlate with each other, which has not been reported yet for the joint application of these techniques to the study of drying paint coatings (Section 4.C). It is worth noting that although our study is restricted to the analysis of solvent-based paints, the employed methods would also be applicable for characterization of different kinds of paints [4].

2. THEORETICAL BACKGROUND

A. Dynamic Speckle

Speckle patterns are known to possess information about the surface of an object at a scale below that of the wavelength used [11,12]. The variation of a speckle pattern with time, i.e., a dynamic speckle pattern, allows further analysis of the object in the temporal domain. The degree of activity of the speckle pattern is usually called SA, as mentioned before.

SA was analyzed through a simple method that counts the average fraction of pixels whose intensities $I(i,j)$ change as a function of time by more than a certain amount, r, called *speckle noise*. The details of this method are described in [13], and here we show its basic equation, which reads

$$\mathrm{SA} = \frac{1}{m \times n} \sum_{k=1}^{N-1} \frac{1}{N-1} \sum_{i=1}^{m} \sum_{j=1}^{n} \Theta[|I_{k+1}(i,j) - I_k(i,j)| - r], \tag{1}$$

where N is the number of images from which a single SA value should be determined, I_k is the kth image, m and n are the image sizes, and $\Theta(x)$ is the well-known Heaviside function. Each SA value calculated through Eq. (1) corresponds to an average activity over a temporal extension $\Delta\tau = (N-1)\tau$, with τ being the elapsed time between images.

B. Holographic Interferometry

The DHI technique consists in the interferometric comparison of numerically reconstructed phase information from two digital holograms. A digital hologram is a digitized image (acquired by a CCD or CMOS sensor) of the unfocused interference map between two coherent wavefronts, namely, (i) a reference wavefront impinging directly onto the digital sensor and (ii) a wavefront reflected off the object under analysis (object wavefront). A hologram contains information about the three-dimensional (3D) shape of the object [14], which can be reconstructed numerically (amplitude + phase) as follows. Given two digital holograms of an object, $h_r(x,y)$ and $h_l(x,y)$, in a reference state (r subscript) and a loaded or perturbed state (l subscript) and a typical off-axis lensless digital Fourier holographic arrangement (see [15] and [16] for details), the reconstruction of point-wise phase differences between both states proceeds as [14]

$$\Delta\phi(\xi,\eta) = \tan^{-1}\left\{\frac{\mathrm{Im}[H_l(\xi,\eta)H_r^*(\xi,\eta)]}{\mathrm{Re}[H_l(\xi,\eta)H_r^*(\xi,\eta)]}\right\}. \tag{2}$$

Here, $H_i(\xi,\eta) \propto \mathrm{FFT}^{-1}[h_i(x,y)]$ is the Fresnel–Kirchhoff backpropagated field at each object state ($i = r, l$), (ξ,η) are the coordinates on the object plane, (x,y) are the coordinates on the hologram plane, Im[·] and Re[·] are the imaginary and real parts, and the asterisk (*) stands for complex conjugate [14]. This operation yields a wrapped phase difference matrix with values in the range $[-\pi,\pi]$ that are related to the object displacement or deformation by

$$\Delta\phi(\xi,\eta) = \mathbf{S}(\xi,\eta) \cdot \mathbf{d}(\xi,\eta). \tag{3}$$

The vector $\mathbf{S}$ (called the *sensitivity* vector) is determined by the experimental setup and can be optimized for displacements or deformations in the desired direction. In this way, the displacement vector $\mathbf{d}$ is given by the real point-wise deformation of the object and can be calculated from Eq. (3) once $\Delta\phi$ is known.

3. EXPERIMENTAL DETAILS

Our experiments consisted in analyzing the evolution of the drying process of a red solvent-based synthetic enamel by means of both SA and DHI measurements. For this, we implemented a typical off-axis lensless Fourier digital holographic arrangement with He–Ne laser illumination and a 5 megapixel CMOS camera (2592 × 1944 pixels). Also, a 1 megapixel CMOS camera (1284 × 1024 pixels) with a focusing lens was used for recording speckle images formed right on the surface of the painted region. A simplified scheme of the experimental setup is shown in Fig. 1.

We analyzed two different cases, namely, (i) a drying paint droplet deposited onto a horizontal surface, so as to avoid flowing and have a definite shape, and (ii) a painted region on a vertical surface, so as to allow free flowing due to gravity and observe painted regions differing in thickness. Specific details of image acquisition parameters are given below for each experience.

4. RESULTS AND DISCUSSION

A. Drying Time Estimation by Dynamic Speckle Measurements

We deposited a small droplet of solvent-based enamel onto a horizontal surface, and it was left to dry at room temperature while speckle and holographic images were acquired.

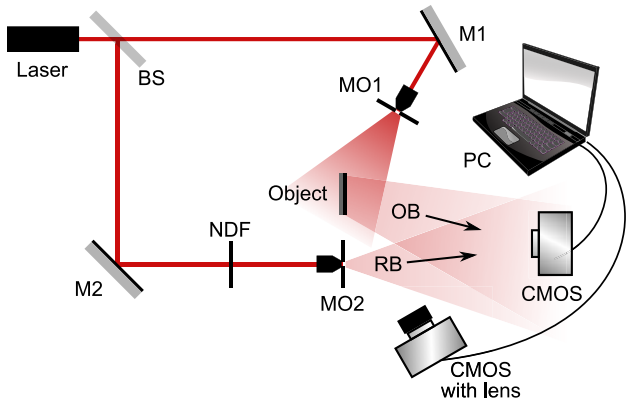

Fig. 1. Simplified diagram of the experimental digital off-axis lensless Fourier holographic arrangement with a second CMOS camera with a lens to acquire the sequence of speckle images. Laser, He–Ne; BS, beam splitter; *Mi*, mirrors; NDF, neutral density filter; *MOi*, microscope objectives and pinholes; OB, object beam; RB, reference beam; CMOS, digital cameras.

In Fig. 2(a) we show the time evolution of SA obtained from the drying droplet. Each point of the curve was calculated from 10 consecutive images acquired each second (i.e., with parameters $N = 10$ and $\tau = 1$ s). The initially linear decaying shape of the curve evidenced the drying process. It is worth noting here the well-known fact that the resulting SA curves for drying paint coatings will follow a linear or logistic decaying trend [2–4,7,13].

After about 90 min the curve in Fig. 2(a) reached a constant SA value of 0.3, which corresponded to the speckle noise value. Background speckle noise is due to many causes, like vibrations, electronic noise, and spurious reflections, and can be estimated before the experiment by performing a test measurement of an unpainted (thus, static) surface, or, otherwise, it can be estimated during the experiment by calculating the SA both on the region of interest and simultaneously on an unpainted or static region of the acquired images.

In this way, drying time can be estimated in a real-time fashion by fitting SA data points to a known function as soon as they are calculated from the acquired speckle images. Therefore, for the data curve of the drying droplet [Fig. 2(a)], the estimation of drying time results directly from performing a direct linear extrapolation to the time axis and correcting the result by considering the background noise value (i.e., extrapolating to the SA background noise line). The solid line in Fig. 2(a) represents the best linear fitting to the data points obtained during the first 70 min of observation. As can be seen, the linear fitting is only meaningful until this observation time of 70 min, since the curve then departs from the linear behavior to reach the background noise level.

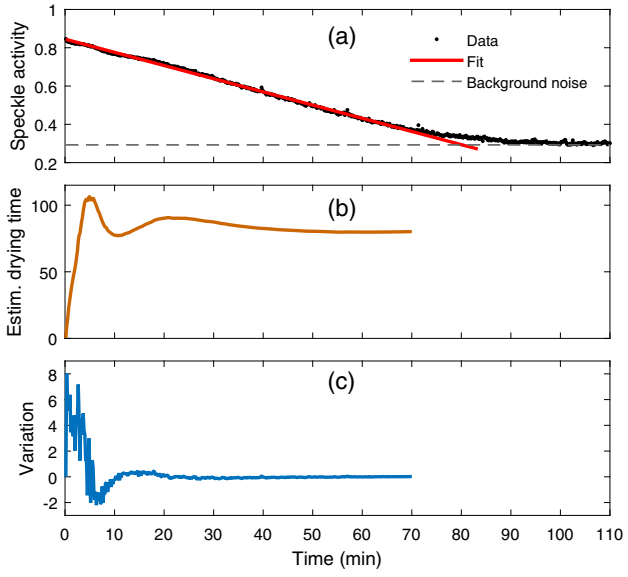

Fig. 2. Time evolution of (a) the SA for a paint droplet on an horizontal surface while drying in ambient conditions, (b) the estimated drying time (in min) by fitting of the SA experimental data, and (c) variation (in min) between consecutive estimated drying times. Linear fit (solid line) in (a) corresponds to data points acquired until 70 min of observation time. Thus, the curves in (b) and (c) were only calculated during this period, since the curve then departs from linear behavior.

The curve shown in Fig. 2(b) presents the evolution of the estimated drying time values (in min), obtained from the least-squares linear regression of the data points as they were acquired (and correcting due to background noise). The estimated drying time converged at a final value of 79 min. However, a quite steady behavior was achieved between 20–30 min of observation. This is evidenced by the end of the oscillations in the curve in Fig. 2(b) and also in the curve in Fig. 2(c), which depicts the variation (in min) from one estimated drying time to the next one.

In this particular experience, we observed that after an observation time of 15 min the predicted drying time values lay inside a ±12% region with respect to the final value of 79 min. Therefore, drying time can be estimated by simple SA data fitting with moderate precision after short observation times, as compared to the time needed for the paint to reach the tack-free state (i.e., 2 h, as already mentioned). It is worth noting that quality and confidence of the fitting will strongly and exclusively depend on each particular case of study.

As an example of this, Fig. 3(a) shows the SA evolution of the vertical painted surface of our second experiment. The curve shape followed a typical smooth logistic decaying function. Each point was obtained from Eq. (1) with $N = 10$ images acquired each $\tau = 5$ s. Therefore, in this case, a logistic function of the form $f(t) = (M - m)/[1 + (t/t_0)^p] + m$ was fitted to experimental SA data by a least-squares regression as speckle images were acquired. The parameters M and m correspond to maximum and minimum values of the function, p determines the decaying rate, and t_0 corresponds to the time position of the curve's inflection (middle) point. The parameter m represents the background speckle noise and does not need to be known previously or measured simultaneously, as in the previous case, since it emerges directly from the fitting

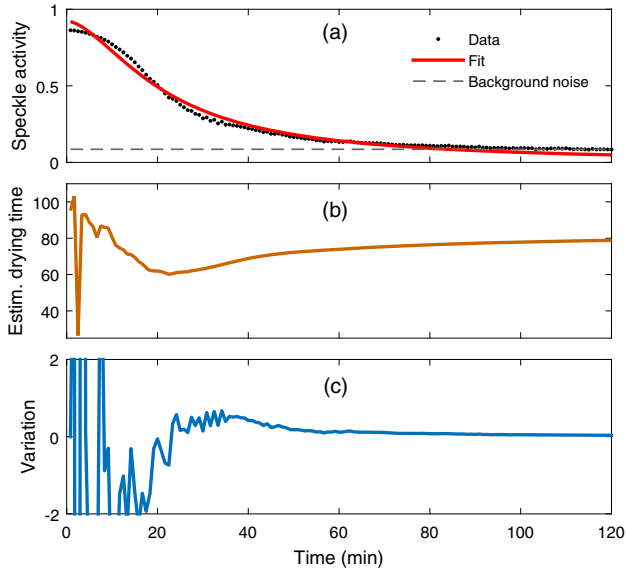

Fig. 3. Time evolution of (a) the SA for a painted vertical surface while drying in ambient conditions, (b) the estimated drying time (in min) by fitting of the SA experimental data, and (c) variation (in min) between consecutive estimated drying times. The logistic (solid line) curve in (a) represents the best fit to all data points.

procedure. The solid line curve in Fig. 3(a) represents the logistic function that best fits the whole set of experimental points. It is clear that here, a linear extrapolation to the time axis would not lead to a correct estimated drying time, since the curve decays asymptotically to the background noise level. Hence, to make adequate comparisons with the previous case of the drying droplet, we have estimated drying time by determining the time for which the fitting function was above the background noise level (or m value) as much as the SA curve in Fig. 2(a) was above the background noise for the corresponding estimated drying time in that case.

By inspecting the experimental SA data in Fig. 2(a), we observed that at the estimated drying time of 79 min the SA value was above the SA background level by an amount of about 0.05. Thus, we took as the estimated drying time, in this second case, the time for which the fitted logistic function was 0.05 above the background SA value, given by the m parameter.

The results of drying time estimation for the painted vertical surface are presented in Figs. 3(b) and 3(c), which respectively show the time evolution of the estimation (in minutes) and its point-to-point variation (in minutes) as SA data points were calculated. An almost steady estimated drying time value was obtained after a similar observation time to the one before, about 30 min, finally converging at 78 min after the whole observation period of 120 min. Remarkably, although both studied cases involved quite different situations with considerably different SA background levels, the drying time estimation yielded almost the same result. This fact is not trivial and gives a clue to a well-known problem of dynamic speckle measurements, regarding the difficulty of getting and objectively quantifying the SA from dynamic speckle patterns [8,13,17]. The similarity between the estimated drying times for the same paint coating in two quite different situations [evidenced by comparing the data curves in Figs. 2(a) and 3(a)] leads us to think that differences between SA and background noise SA values correctly represent the drying state of the paint coating.

Despite the differences observed between the two cases presented, regarding the decaying trend (linear or logistic) of the SA, the shape of the resulting curve will be one or the other, as has already been reported by many authors [2–4,7,13]. Therefore, the algorithm used for the fitting procedure would just have to include a simple routine to determine whether the data collected should be fitted with a linear or a logistic function. Moreover, after suitable calibration procedures, depending on each particular application, one could find, in principle, a method that correctly detects the drying state of the paint coating, as described above.

B. Thickness Variation Determination of Drying Paint Coatings by DHI

As we already mentioned, DHI allows us to analyze point-wise morphological variations throughout the surface of several kinds of samples. In particular, we have not found in the literature an analysis of thickness variations in drying paint coatings, which would also yield valuable information about the drying process. In the following, we show the results obtained after implementing DHI measurements to determine morphological variations of the drying paint during both studied cases.

In Fig. 4(a) we show a sequence of interferograms obtained from the drying droplet. During the first stages of the process, the paint remains in a liquid state, and coating variations between successive holograms are too large and nonhomogeneous, which means the information extracted from those interferograms is not useful to quantify thickness variations. However, once the coating surface reaches some degree of stiffness, the interferograms allow us to follow the variations in its morphology. In our case, the paint achieved this state after about 45 min. The first (top) image of the sequence in Fig. 4(a) was the first interferogram showing a distinguishable phase structure. Each image in this sequence was separated from the next by a time lapse of 150 s, which yielded a total time from top to bottom of 27.5 min. This evidenced a slow drying process. The last interferograms showing noticeable phase variations (not shown here) were obtained after a drying time of about 100 min. This is in very good agreement with the SA curve in Fig. 2(a), since there the background noise level was also achieved after about 100 min. In turn, Fig. 4(b) presents a simplified diagram of the evolution of the droplet shape during the drying process. This illustrates how phase variations observed in the interferograms can be directly related to shape, thickness, or height variations (Δz) in the droplet surface. As seen in Fig. 4(b), Δz would be higher at the center of the droplet, which is in accordance with the observed phase map sequence in Fig. 4(a).

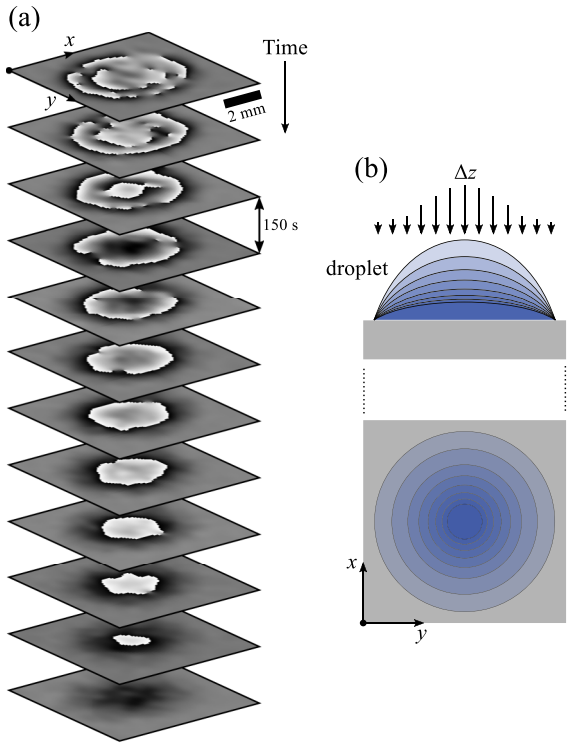

Fig. 4. (a) Sequence of interferograms obtained for an intermediate stage of the droplet drying process (starting after about 45 min of paint application). The time period between consecutive interferograms is 150 s, which yields a total time from top to bottom of 27.5 min. (b) Scheme illustrating side and top views of thickness variations (Δz) during paint drying.

Figures 5(a) and 5(b) show the reconstructed information of the morphological variations in the droplet after unwrapping and integrating the phase values extracted from consecutive interferograms and converting them to physical displacements of the coating surface.

We have integrated the unwrapped phase map values starting from about 45 min, as mentioned above, since before that time the paint did not reach a sufficiently stiff surface state and the information recovered was not useful. The 3D map in Fig. 5(a) accounts for the total displacement Δz calculated for each surface point of the drying droplet, and has a Gaussian-like shape that is in agreement with the expected behavior shown in Fig. 4(b). A maximum value of 51 μm was obtained for the central point, as expected. Figure 5(b) presents the same morphological information as Fig. 5(a), but in the form of a 2D contour plot, which allows for a more precise analysis of regions with different Δz values. Through an analysis of the evolution of phase values in a region located near the droplet that should not change with time, we determined the relative errors introduced in the determination of Δz values, which were below 3.8%.

In Figs. 6(a)–6(c) we present the results obtained after an analogous morphological analysis of the paint coating while drying onto a vertical surface. For comparison purposes, we have integrated the phase variations extracted from interferograms during the same period of time in both cases (i.e., from 45 to 120 min of observation).

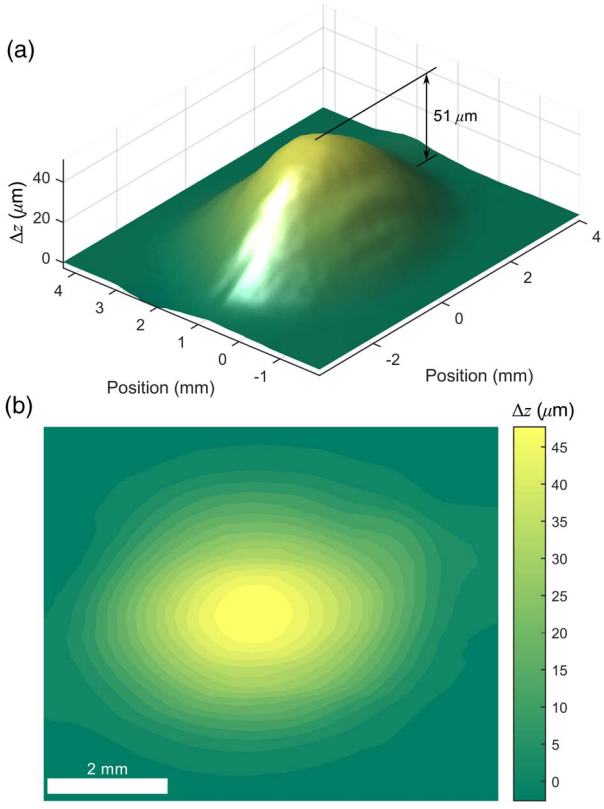

Fig. 5. Reconstruction of the morphological changes in the drying droplet seen in (a) 3D perspective and (b) a contour level graph. The vertical axis in (a) and the color scale in (b) represent point-wise thickness variations of the droplet surface.

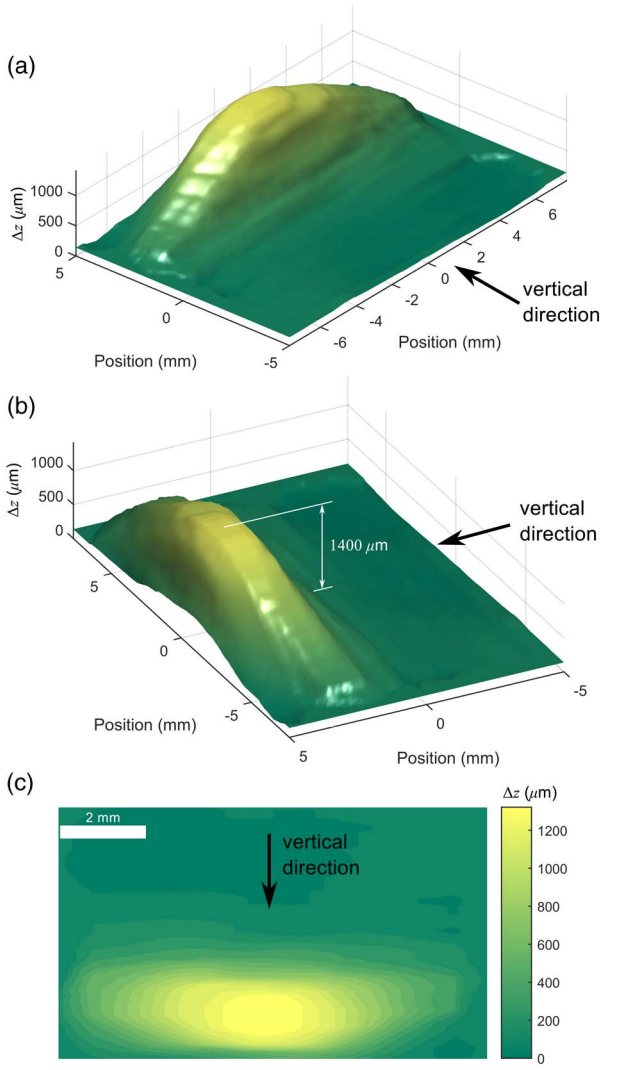

Fig. 6. Reconstruction of the morphological changes in the drying paint coating on a vertical surface in (a), (b) two different 3D perspectives and (c) a contour level graph. The vertical axis in (a) and (b) and the color scale in (c) represent point-wise thickness variations of the coating.

As expected, due to flowing after application, an accumulation of the paint at the bottom of the coated surface was observed, as is clearly seen from two different perspectives in the 3D maps in Figs. 6(a) and 6(b). A larger thickness variation of about 1400 μm was also observed, centered horizontally in the coated region. This is similar to the case of the droplet, where larger thickness variations occurred toward the middle of the covered region and smaller ones toward the borders. We attribute this to the effect of surface tension. Figure 6(c) presents the same information, but as a contour level plot.

The considerable difference in overall thickness variations between both cases (with a maximum value of 51 μm against 1400 μm for the droplet and the vertical surface, respectively) is due to the fact that the droplet dried statically (i.e., without paint flowing), while on the vertical surface the paint rapidly flowed and accumulated at the bottom of the surface prior

to drying. We could verify this by simple visual inspection during the experiments.

C. Correlations between Dynamic Speckle and DHI Measurements and Corrections to Drying Time Estimation

As mentioned in the above discussion (Section 4.B), the first observed correlation between dynamic speckle and DHI measurements corresponded to the evidence that the last interferograms showing noticeable phase variations (in the case of the droplet) were obtained after a drying time of about 100 min. This is in very good agreement with the fact that the SA curve in Fig. 2(a) also reached the background noise level after 100 min of observation.

To further analyze correlations between both techniques, we sought a way to measure some kind of decaying activity curves from the information contained in the interferograms, so as to compare them with the SA curves obtained from dynamic speckle measurements. We found that a possible and simple way was to analyze the evolution of the area fraction showing thickness variations between consecutive interferograms (the active area fraction, going forward). We show below the results obtained from this analysis.

At the top of Figs. 7(a) and 7(b) we show a sequence of interferograms for both studied cases, i.e., (a) the droplet on a horizontal surface and (b) the vertical painted surface. Both sequences proceed from left to right and show interferograms equally spaced in time, from the beginning to the end of the drying process in each case. The diminution of the active area fraction along the extension of drying coating is evident. As can be seen in Fig. 7(a), the unpainted regions around the drying droplet have a gray color in the interferograms, corresponding to a zero phase change between two consecutive holograms. In turn, regions having a speckle-type texture (at the beginning of the process) or fringes (toward the end of the process) are active zones that present variations between holograms. Consequently, as the drying process advances, all points in the interferograms will finally turn into a homogeneous gray color. Therefore, the active area fraction can be easily estimated by simply counting the fraction of pixels that presented phase variations in each interferogram. In turn, the bottom graphs of Figs. 7(a) and 7(b) show the curves obtained for the active area fraction, which presented a logistic shape, as expected.

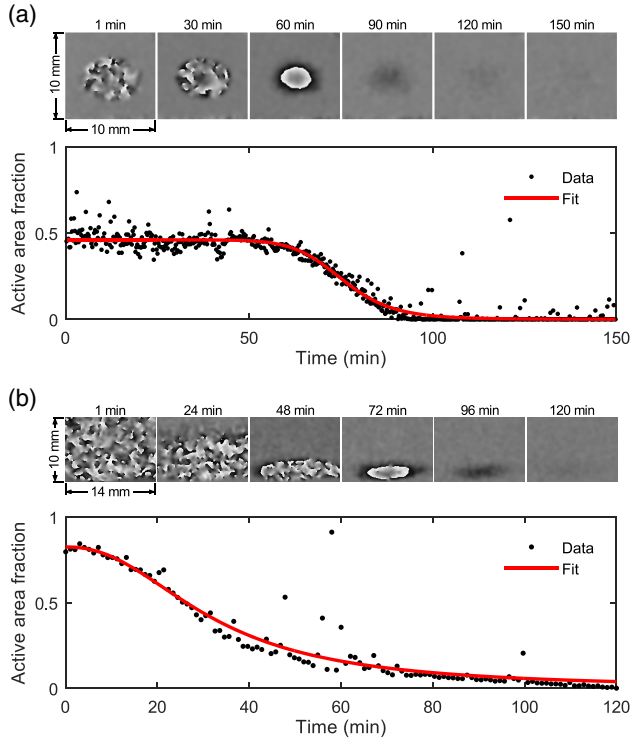

Fig. 7. Sequences of interferograms and active area fraction curves for (a) the droplet drying on a horizontal surface and (b) the vertical painted surface. Regions with a homogeneous gray color in each image correspond to static or already dried zones, while active zones present a speckle-type texture or fringes. The dimensions shown agree with those in Figs. 5 and 6.

In Figs. 8(a) and 8(b) we compare the evolution of the active area fraction with that of the SA values in Figs. 2 and 3, respectively. As seen in Fig. 8(a), despite both curves having different shapes (linear and logistic) during the first 60 min, they decay to zero after almost the same time (about 100 min). Moreover, the active area fraction starts to decay after about 60 min, in accordance with the time for which the SA curve departs from a linear behavior.

In turn, the curves obtained for the paint drying on the vertical surface are much more similar, as seen in Fig. 8(b). They present almost the same logistic behavior, also decaying to zero activity after 100 min of observation.

These correlations allow us to conclude that, remarkably, both techniques (dynamic speckle and DHI) detected the end of the drying process at almost exactly the same time (≈100 min) in both experiments. Therefore, from these results, one can decide to take as a better drying time estimation the time for which both the SA and active area fraction normalized curves (after data fitting) decay to zero, or, rather, below some positive value. This latter fact is important, since it

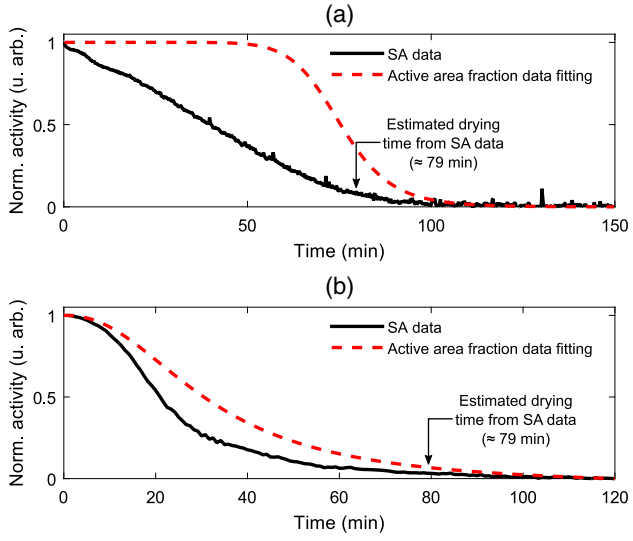

Fig. 8. Comparison between the curves fitted to the active area fraction data points (dashed lines), obtained by DHI, and the measured SA values (solid lines) for (a) the drying droplet and (b) the painted vertical surface cases. Estimated drying time from SA data in each case is shown with the arrows.

introduces a degree of freedom or calibration factor between the optically estimated drying time (noninvasive method) and the time needed for the paint to achieve a tack-free state, which is evidenced manually by just touching the paint (invasive method).

5. CONCLUSION

In summary, we have shown how both dynamic speckle and DHI techniques can be implemented at the same time to characterize the drying process of a solvent-based paint coating. We note that the methods described would also be applicable to different kinds of paints, as mentioned before. With dynamic speckle, we have predicted, after a relatively short observation period, the drying time of the coating through the fitting of the experimental SA curve. The time needed to achieve a minimum degree of confidence on the drying time prediction will depend to some extent on each particular case of study. However, the advantage of the dynamic speckle technique is that the *a priori* known decaying trend of the SA for drying paint will, in general, allow us to predict the drying time after an observation period much shorter (of about 20–30 min) than the time the paint needs to reach the so-called tack-free state (≈2 h for solvent-based paints). In turn, by exploiting the high sensitivity of DHI, we performed a morphological analysis to map the evolution of thickness variations in the coating surface with relative uncertainties below 3.8%. Finally, we analyzed the correlation between the results obtained from both techniques. For this, from the interferograms obtained we determined the evolution of the active area fraction of the drying coating surface, i.e., the area fraction of the coating that presented thickness variations between consecutive holograms. The time evolution of active area fraction presented a similar behavior to that of the SA values, which enabled us to detect correlations between both techniques. Notably, we observed that dynamic speckle and DHI detected the end of the drying process at almost the same time (after ≈100 min of observation). This fact, which has not been reported previously in the literature to our knowledge, allowed us to conclude that by combining both techniques, a better drying time estimation can be achieved. Therefore, the results presented in this work contribute to scientific, industrial, and applied research fields regarding the characterization, synthesis, manufacture, and application of different kinds of paint coatings.

Funding. ANPCyT (PICT 2013-1034); CONICET.

REFERENCES

1. M. Yokota, T. Kawakami, Y. Kimoto, and I. Yamaguchi, "Drying process in a solvent-based paint analyzed by phase-shifting digital holography and an estimation of time for tack free," Appl. Opt. **50**, 5834–5841 (2011).
2. J. I. Amalvy, C. A. Lasquibar, R. Arizaga, H. Rabal, and M. Trivi, "Application of dynamic speckle interferometry to the drying of coatings," Prog. Org. Coat. **42**, 89–99 (2001).
3. M. Z. Ansari and A. K. Nirala, "Following the drying process of Fevicol (adhesive) by dynamic speckle measurement," J. Opt., doi:10.1007/s12596-015-0298-x to be published).
4. P. A. Faccia, O. R. Pardini, J. I. Amalvy, N. Cap, E. E. Grumel, R. Arizaga, and M. Trivi, "Differentiation of the drying time of paints by dynamic speckle interferometry," Prog. Org. Coat. **64**, 350–355 (2009).
5. I. Yamaguchi, M. Yokota, T. Ida, M. Sunaga, and K. Kobayashi, "Monitoring of paint drying process by digital speckle correlation," Opt. Rev. **14**, 362–364 (2007).
6. A. Mavilio, M. Fernández, M. Trivi, H. Rabal, and R. Arizaga, "Characterization of a paint drying process through granulometric analysis of speckle dynamic patterns," Signal Process. **90**, 1623–1630 (2010).
7. E. Blotta, V. Ballarín, M. Brun, and H. Rabal, "Evaluation of speckle-interferometry descriptors to measuring drying-of-coatings," Signal Process. **91**, 2395–2403 (2011).
8. J. Moreira, R. R. Cardoso, and R. A. Braga, "Quality test protocol to dynamic laser speckle analysis," Opt. Laser Eng. **61**, 8–13 (2014).
9. G. Sheoran, S. Sharma, and C. Shakher, "Monitoring of drying process and cracking/disbonding of paints using lensless Fourier transform digital holography," Opt. Lasers Eng. **49**, 159–166 (2011).
10. M. Guzman, G. J. Meschino, A. L. Dai Pra, M. Trivi, L. I. Passoni, and H. Rabal, "Dynamic laser speckle: decision models with computational intelligence techniques," Proc. SPIE **7387**, 738717 (2010).
11. H. J. Rabal and R. A. Braga, Jr., *Dynamic Laser Speckle and Applications* (CRC Press, 2009).
12. C. A. Paixão and A. T. da Costa, "Dynamic model for biospeckle," J. Opt. Soc. Am. A **30**, 1089–1098 (2013).
13. N. Budini, C. Mulone, F. M. Vincitorio, C. Freyre, A. J. López, and A. Ramil, "Two simple methods for overall determination of mobility in dynamic speckle patterns," Optik **124**, 6565–6569 (2013).
14. T. Kreis, *Handbook of Holographic Interferometry* (Wiley, 2005).
15. J. L. Valin, E. Gonçalves, F. Palacios, and J. R. Pérez, "Methodology for analysis of displacement using digital holography," Opt. Lasers Eng. **43**, 99–111 (2005).
16. N. Budini, C. Mulone, F. M. Vincitorio, A. J. López, and A. Ramil, "Analysis of small deflections by double-exposure digital holographic interferometry," in *IEEE Biennial Congress of Argentina (ARGENCON)*, Bariloche, Argentina (2014), pp. 428–432.
17. M. A. Montecinos, V. M. Canales, N. Cap, E. Grumel, H. Rabal, M. Trivi, and E. Baradit, "Evaluation of activity images in dynamics speckle in search of objective estimators," Proc. SPIE **9660**, 96601Z (2015).